JOURNAL OF COMPUTATIONAL PHYSICS 104, 303–312 (1993)

A Chebyshev–Legendre Spectral Method for the Transient Solutions of Flow Past a Solid Sphere

HOA D. NGUYEN

Idaho National Engineering Laboratory, EG & G Idaho, Inc., Idaho Falls, Idaho 83415

AND

JACOB N. CHUNG

Department of Mechanical and Materials Engineering, Washington State University, Pullman, Washington 99164

Received July 17, 1991; revised April 21, 1992

A full spectral model for the stream-function-vorticity formulation is developed for the solution of unsteady flow past a rigid sphere. To convert the governing partial differential equations to discrete form, Chebyshev and Legendre polynomials are employed to expand the vorticity and stream function in the radial and angular directions, respectively, together with a first-order, fully implicit, iterative scheme for time advancement. The solution to the system of discrete nonlinear equations is accomplished by LU decomposition in conjunction with the influence matrix to resolve the lack of vorticity boundary conditions. Owing to the global nature of the orthogonal trial functions, the present technique provides a means to achieve highly accurate results with less number of unknowns than either traditional finite difference or finite element methods. Comparisons of numerical solutions with previous results show consistent trends as reported in studies dealing with Cartesian coordinates.

1. INTRODUCTION

Finite difference (FDM) and finite element (FEM) methods have been among the traditional numerical techniques for simulating a wide variety of engineering and/or scientific problems. However, the newly emerged branch of numerical methodology, herein referred to as spectral method (SM), has generated much interest in recent years, particularly amongst those working in the areas of fluid dynamics and heat/mass transfer. The increased popularity is partly due to the successful development of an approach that links SM to the well developed fast transforms such as FFT (fast Fourier transform, of which Chebyshev's is a special case), which makes the computations efficient. According to the survey of Fletcher [1], the main weakness of SM relative to FDM and FEM is its inflexibility to be adaptable to irregular computational domain, but since the appearance of spectral element models that combine the generality of FEM and the accuracy of SM, this weakness seems to be improved [2].

The basic idea of SM is to express the dependent variables in the form of a series of orthogonal functions with unknown coefficients. The trial functions which commonly used in spectral expansion include the Chebyshev, Legendre, and Laguerre polynomials for problems involving nonperiodic boundary conditions, and Fourier series otherwise. The unknown coefficients can be found by various criteria as described by Finlayson, see Ref. [3]. In the pseudo-spectral method (PSM), the criteria is to make the solution error-free at the collocation points; hence, the solution becomes exact in the limit as the number of collocation points increases. Ku and Hatziavramidis [4] applied the concept to a two-dimensional steady flow in a cavity driven by a moving lid and confirmed the superiority of PSM over FDM as far as accuracy and efficiency are concerned. To be specific, PSM needs 13×13 and 25×15 nodal points, whereas FDM requires a grid system containing 121×121 and 141×141 nodes for Reynolds numbers of 100 and 200, respectively, in order to achieve the same resolutions [4]. In the same study but different flow configuration, Ku and Hatziavramidis found an exceptional agreement between their axial velocity of pipe flow with existing data [4]. There have been numerous spectral versions of various degree of complexity, but the majority of those models are only applicable as long as the computational domain is bounded by simple boundaries. Interested readers are suggested to consult Canuto *et al.* [3] for a comprehensive and up-to-date review in this area.

The objectives of this study are two-fold. First, a full spectral model that employs the Chebyshev and Legendre polynomials as the basis trial functions is developed and applied to the stream-function-vorticity formulation for computing the transient flow around a stationary sphere at low and

0021-9991/93 $5.00

intermediate Reynolds numbers. According to our literature survey, pioneering efforts in the spectral methods for this flow geometry can be traced back the work of Dennis and Walker [5], where a partial spectral model that combines FDM and SM was used. Their results, based on the Legendre expansion along with FDM to approximate angular and radial derivatives, respectively, demonstrated a remarkable success in predicting the steady flow patterns for Reynolds numbers up to 40. In a series of subsequent papers, their hybrid spectral version was extended to flow generated by a sphere under spinning motion [6], to a transient flow field developed following an impulsive start [7], and to a rotating boundary layer flow [8]. Recent theoretical analysis showed that the convergence rate associated with the SM behaves in an exponential fashion in contrast to $(1/N)^m$ for FDM and FEM methods, with N and m being the number of nodal points and order of the scheme, respectively [3]. In an attempt to recover the loss of accuracy due to FDM in early spectral schemes, this paper proposes the use of Chebyshev collocation in the radial direction, and such modification when used in parallel with the Legendre expansion in the angular direction would constitute a full spectral scheme. Second, the influence matrix technique is incorporated into the spectral model to handle the lack of vorticity conditions along the boundaries due to the overspecification of boundary conditions for the stream function. Such treatment eliminates the need of asymptotic condition for the vorticity at large distance from the sphere.

2. GOVERNING EQUATIONS

As usual, the flow of an isothermal, Newtonian fluid at any instance in time is described by the Navier–Stokes equations. These equations are found to be especially useful when written in terms of vorticity and stream function. For axisymmetric, incompressible flow, the equations can be recast into the dimensionless system of equations,

$$\frac{\partial \Omega}{\partial t} - \frac{1}{r}\frac{\partial(\Psi, \Omega/r\sin\theta)}{\partial(r,\theta)} = \frac{2}{\mathrm{Re}}\frac{1}{r\sin\theta}E^2(\Omega r\sin\theta), \quad (1)$$

$$E^2\Psi = -\Omega r\sin\theta, \quad (2)$$

where the radial coordinate has been non-dimensionalized by the sphere radius R, the time t by R/U_∞, the stream function Ψ by R^2U_∞, and the vorticity Ω by U_∞/R. Also θ is the angular coordinate measured from the backward stagnation point, Re is the Reynolds number based on the sphere diameter and the droplet velocity U_∞, and $\partial(\ ,\ )/\partial(\ ,\ )$ is the conventional notation of the Jacobian. The operator E^2 employed in Eqs. (1) and (2) has been defined as

$$E^2 \equiv \frac{\partial^2}{\partial r^2} + \frac{\sin\theta}{r^2}\frac{\partial}{\partial\theta}\left(\frac{1}{\sin\theta}\frac{\partial}{\partial\theta}\right). \quad (3)$$

Since the stream function is defined in such a way that the continuity equationis satisfied, we can write the radial and tangential velocity components U_r and U_θ, non-dimensionalized by U_∞, as follows:

$$U_r = \frac{1}{r^2\sin\theta}\frac{\partial\Psi}{\partial\theta}, \quad U_\theta = \frac{-1}{r\sin\theta}\frac{\partial\Psi}{\partial r}. \quad (4)$$

To complete the mathematical formulation, we specify the boundary conditions in accordance with the following requirements: First, the flow field is assumed to be undisturbed by the presence of the sphere at distances far from the particle and along the axis of symmetry. Second, the relative velocity between the fluid and the sphere is zero at the surface. These conditions, when translated to mathematical constraints, lead to

$$\Psi(t, r, 0) = \Psi(t, r, \pi) = \Omega(t, r, 0) = \Omega(t, r, \pi) = 0, \quad (5)$$

$$\frac{\partial\Psi}{\partial r}(t, 1, \theta) = 0, \quad \Psi(t, 1, \theta) = 0,$$

$$\Psi(t, r\to\infty, \theta) \approx r_\infty^2\int_\mu^1 P_1(\mu^*)\,d\mu^*, \quad (6)$$

where r_∞ is the truncated radius beyond which the flow is approximately uniform, P_1 is the Legendre polynomial of order 1, and μ is $\cos\theta$.

The initial conditions considered in this work are given as

$$\Psi(0, r, \theta) = \Omega(0, r, \theta) = 0, \quad (7)$$

which correspond to the physical situation that the flow is impulsively started at time $t = 0$.

3. METHOD OF SOLUTION

3.1. *Spectral Representations*

The present spectral method employs Chebyshev and Legendre polynomials as basis functions in the radial and angular directions respectively. As a first step prior to adapting the Chebyshev expansion, we truncate the flow field, originally unbounded, so that the computational domain becomes a spherical shell whose normal distance is further rescaled to $[-1, 1]$. This projection may be accomplished by the use of an exponential mapping which also

offers an adequate resolution in the vicinity of the sphere surface where large velocity gradients exist. The coordinate transformation we use is

$$r = e^{(1-\eta)\,\xi_\infty/2}, \tag{8}$$

where ξ_∞ is an adjusting parameter that controls the truncation of the physical domain. With the newly defined coordinates, the flow variables are expanded as a series of Legendre and its associated polynomials in the form

$$\{\Psi, \Omega\} = \sum_{n=1}^{NL} \{e^{(1-\eta)\,\xi_\infty/4}\Psi_n(t,\eta), \Omega_n(t,\eta)\} \times \left\{\int_\mu^1 P_n(\mu^*)\,d\mu^*, P_n^1(\mu)\right\}, \tag{9}$$

in which NL is the number of terms to be included in the series and $P_n^k(\mu)$ is the Legendre polynomial of the kth kind and order n. By making the substitution of the stream function and vorticity expansions, and after considerable algebraic manipulation, the governing equations can be recast to a form with no angular dependence,

$$\frac{4}{\xi_\infty^2}\frac{\partial^2\Psi_n}{\partial\eta^2} - \left(n+\frac{1}{2}\right)^2\Psi_n = -e^{5(1-\eta)\,\xi_\infty/4}n(n+1)\,\Omega_n, \tag{10}$$

$$\frac{\partial\Omega_n}{\partial t} = \frac{2}{\mathrm{Re}}\,e^{-(1-\eta)\,\xi_\infty} \times\left[\frac{4}{\xi_\infty^2}\frac{\partial^2\Omega_n}{\partial\eta^2} - \frac{2}{\xi_\infty}\frac{\partial\Omega_n}{\partial\eta} - n(n+1)\,\Omega_n\right] + S_n, \tag{11}$$

where we have made use of the orthogonality properties of Legendre functions along with their recursive formulas. Since these relations can be found in any standard text on special functions, they are omitted here. Despite the fact that the resulting equations are somewhat simpler than the original ones, nonlinearities are still present in the convective acceleration term, given by

$$S_n = e^{-5(1-\eta)\,\xi_\infty/4}\sum_{i=1}^{NL}\sum_{j=1}^{NL}\left\{\alpha_{ij}^n\Psi_i\left(\frac{2}{\xi_\infty}\frac{\partial\Omega_j}{\partial\eta}+\Omega_j\right) + \beta_{ij}^n\Omega_j\left(\frac{2}{\xi_\infty}\frac{\partial\Psi_j}{\partial\eta}-\frac{\Psi_j}{2}\right)\right\}, \tag{12}$$

where α_{ij}^n and β_{ij}^n are constants representing the integrals of products of three associated Legendre functions. Rottenberg *et al.* [9] presented the theory expressing these constants in terms of 3-J symbol, a representation of integral of product of three Legendre functions, and devised algorithms to compute them numerically. Using their notations we have

$$\alpha_{ij}^n = -(2n+1)\left[\frac{j(j+1)}{n(n+1)}\right]^{1/2} \times\begin{pmatrix} n & i & j\\ -1 & 0 & 1\end{pmatrix}\begin{pmatrix} n & i & j\\ 0 & 0 & 0\end{pmatrix}, \tag{13}$$

$$\beta_{ij}^n = (2n+1)\left[\frac{j(j^2-1)(j+2)}{n(n+1)\,i(i+1)}\right]^{1/2} \times\begin{pmatrix} n & i & j\\ -1 & -1 & 2\end{pmatrix}\begin{pmatrix} n & i & j\\ 0 & 0 & 0\end{pmatrix}. \tag{14}$$

Even though successful applications of the FDM to Eqs. (10) and (11) have been made by Dennis and Walker [5] in their computation of steady flow about a spherical particle subjected to a uniform motion, the great potential of the pseudospectral method has motivated us to consider a full spectral model for this problem. In doing so, the vorticity and stream function components in the above equations are replaced by Chebyshev polynomials expansions. Upon enforcement of the solution to be error-free at the collocation points chosen to be the Gauss–Lobatto quadrature points, point, $\cos(i\pi/\mathrm{NT})$, the results are

$$\frac{4}{\xi_\infty^2}\sum_{l=0}^{NT}\hat{G}_{k,l}^{(2)}\Psi_{nl} - \left(n+\frac{1}{2}\right)^2\Psi_{nk} = -e^{5(1-\eta_k)\,\xi_\infty/4}n(n+1)\,\Omega_{nk}, \tag{15}$$

$$\frac{d\Omega_{nk}}{dt} = \frac{2e^{-(1-\eta_k)\,\xi_\infty}}{\mathrm{Re}}\left\{\sum_{l=0}^{NT}\left(\frac{4}{\xi_\infty^2}\hat{G}_{k,l}^{(2)} - \frac{2}{\xi_\infty}\hat{G}_{k,l}^{(1)}\right)\Omega_{nl} - n(n+1)\,\Omega_{nk}\right\} + S_{nk}, \tag{16}$$

where $\hat{G}_{k,l}^{(\chi)}$ is a $(\mathrm{NT}+1)\times(\mathrm{NT}+1)$ Chebyshev derivative matrix of order χ. Although a complete derivation of the derivative matrices is not given here, detailed information can be found elsewhere [4, 10]. In full spectral form, S_{nk} becomes

$$S_{nk} = e^{-5(1-\eta_k)\,\xi_\infty/4}\sum_{i=1}^{NL}\sum_{j=1}^{NL}\left\{\alpha_{ij}^n\Psi_{ik}\left(\frac{2}{\xi_\infty}\sum_{l=0}^{NT}\hat{G}_{k,l}^{(1)}\Omega_{jl}+\Omega_{jk}\right) + \beta_{ij}^n\Omega_{jk}\left(\frac{2}{\xi_\infty}\sum_{l=0}^{NT}\hat{G}_{k,l}^{(1)}\Psi_{il}-\frac{\Omega_{ik}}{2}\right)\right\}. \tag{17}$$

Equations (15) and (16) are nothing more than a system of mixed algebraic and differential equations which can be solved by any of several methods for initial value problems. It is important to note that equations (15) to (17) are now pointwise so that Ψ_{nk} and Ω_{nk} refer to the nth component at the point η_k.

3.2. *Temporal Discretization*

Among the most commonly used time differencing scheme for integrating the spectral equations include the predictor–corrector and the multi-time levels, such as the combined second-order Adams–Bashforth and Crank–Nicolson algorithms. Although these schemes exhibit some desirable features in their own right, their applicability varies widely from problem to problem due to numerical instability arising from the explicitness. In the wake of such potential difficulty, we shall adopt a simple fully implicit scheme which, besides enhancing stability, enables a relatively longer step size,

$$\frac{\mathrm{Re}}{2\Delta t}\Omega_{nk} - e^{-(1-\eta_k)\xi_\infty}\left\{\sum_{l=0}^{\mathrm{NT}}\left(\frac{4}{\xi_\infty^2}\hat{G}_{k,l}^{(2)} - \frac{2}{\xi_\infty}\hat{G}_{k,l}^{(1)}\right)\Omega_{nl} - n(n+1)\,\Omega_{nk}\right\} = \frac{\mathrm{Re}}{2\Delta t}\Omega_{nk}^{*} + \frac{\mathrm{Re}}{2}S_{nk}, \tag{18}$$

where Δt is the time increment and that the superscript * has been used to denote the old time level. Since Eq. (18) is nonlinear, direct solution is out of the question and iterative treatment is necessary. For this reason, we rewrite Eqs. (15) and (18) as

$$\frac{4}{\xi_\infty^2}\sum_{l=0}^{\mathrm{NT}}\hat{G}_{k,l}^{(2)}\Psi_{nl}^{m+1} - \left(n+\frac{1}{2}\right)^2\Psi_{nk}^{m+1} = -e^{5(1-\eta_k)\xi_\infty/4}n(n+1)\,\Omega_{nk}^{m+1}, \tag{19}$$

$$\frac{\mathrm{Re}}{2\Delta t}\Omega_{nk}^{m+1} - e^{-(1-\eta_k)\xi_\infty}\left\{\sum_{l=0}^{\mathrm{NT}}\left(\frac{4\hat{G}_{k,l}^{(2)}}{\xi_\infty^2} - \frac{2\hat{G}_{k,l}^{(1)}}{\xi_\infty}\right)\Omega_{nl}^{m+1} - n(n+1)\,\Omega_{nk}^{m+1}\right\} = \frac{\mathrm{Re}}{2\Delta t}\Omega_{nk}^{*} + \frac{\mathrm{Re}}{2}S_{nk}^{m}, \tag{20}$$

where we have denoted the iteration cycle by the superscript m. To begin the iteration, an initial guess is supplied and from that Eqs. (20) and (19) are solved repeatedly in a successive manner until an asymptotic limit is reached. Criteria for determining convergence is dictated by the rule

$$\left\{\begin{matrix}|\Omega_{nk}^{m+1} - \Omega_{nk}^{m}| \\ |\Psi_{nk}^{m+1} - \Psi_{nk}^{m}|\end{matrix}\right\} \leqslant \{\varepsilon\}, \quad \forall\, n, k, \tag{21}$$

where $\{\varepsilon\}$ is the prescribed tolerance vector. Though Eqs. (19) and (20) are linear and can be solved easily, the absence of vorticity boundary conditions requires a special attention. In the next section, we shall discuss a procedure which decouples the stream function and the vorticity transport equations as well as alleviates the difficulties arising in vorticity–stream function formulation.

3.3. *Vorticity/Stream Function Decomposition*

The key element of this method is to decompose the vorticity and stream function such that all the constraints on the stream function are satisfied simultaneously, and at the same time vorticity boundary conditions, are resolved [11–13]. For the present problem, we consider the decomposition

$$\left\{\begin{matrix}\Psi_n^{m+1} \\ \Omega_n^{m+1}\end{matrix}\right\} = \left\{\begin{matrix}\psi_0 \\ \omega_0\end{matrix}\right\} + \gamma_1\left\{\begin{matrix}\psi_1 \\ \omega_1\end{matrix}\right\} + \gamma_2\left\{\begin{matrix}\psi_2 \\ \omega_2\end{matrix}\right\}, \tag{22}$$

where the expansion functions are the solutions of the following supplementary problems:

$$\left.\begin{aligned}&\frac{\mathrm{Re}}{2\Delta t}\omega_{ik} - e^{-(1-\eta_k)\xi_\infty}\left[\sum_{l=0}^{\mathrm{NT}}\left(\frac{4\hat{G}_{k,l}^{(2)}}{\xi_\infty^2} - \frac{2\hat{G}_{k,l}^{(1)}}{\xi_\infty}\right)\omega_{il} - n(n+1)\,\omega_{ik}\right] = 0 \\ &\frac{4}{\xi_\infty^2}\sum_{l=0}^{\mathrm{NT}}\hat{G}_{k,l}^{(2)}\psi_{il} - \left(n+\frac{1}{2}\right)^2\psi_{ik} = -e^{5(1-\eta_k)\xi_\infty/4}n(n+1)\,\omega_{ik}\end{aligned}\right\}, \quad i = 1, 2. \tag{23}$$

The boundary conditions which go along with the system (23) are specified as

$$\begin{gathered}\omega_i(\eta = 1) = \delta_{i2}, \quad \omega_i(\eta = -1) = \delta_{i1}, \\ \psi_i(\eta = \pm 1) = 0, \quad i = 1, 2,\end{gathered} \tag{24}$$

where δ_{ij} is the Kronecker delta. Unlike the above auxiliary functions, the remaining one satisfies exactly the same equation, but with the right-hand-side replaced by that of the original Eq. (20), i.e.,

$$\left.\begin{aligned}&\frac{\mathrm{Re}}{2\Delta t}\omega_{0k} - e^{-(1-\eta_k)\xi_\infty}\left[\sum_{l=0}^{\mathrm{NT}}\left(\frac{4\hat{G}_{k,l}^{(2)}}{\xi_\infty^2} - \frac{2\hat{G}_{k,l}^{(1)}}{\xi_\infty}\right)\omega_{0l} - n(n+1)\,\omega_{0k}\right] = \frac{\mathrm{Re}}{2\Delta t}\Omega_{nk}^{*} + \frac{\mathrm{Re}}{2}S_{nk}^{m} \\ &\frac{4}{\xi_\infty^2}\sum_{l=0}^{\mathrm{NT}}\hat{G}_{k,l}^{(2)}\psi_{0l} - \left(n+\frac{1}{2}\right)^2\psi_{0k} = -e^{5(1-\eta_k)}\,\xi_{\infty\infty/4}n(n+1)\,\omega_{0k}\end{aligned}\right\}, \tag{25}$$

along with the boundary conditions which can easily be derived from the problem formulation. Thus,

$$\omega_0(\eta = \pm 1) = 0, \quad \psi_0(\eta = 1) = 0, \quad \psi_0(\eta = -1) = e^{3/2\xi_\infty}\delta_{nl}. \tag{26}$$

By imposing the requirements that the stream function

give the correct value of the derivative at the end points, we must have

$$\begin{bmatrix} \psi_1'|_{\eta=1} & \psi_2'|_{\eta=1} \\ \psi_1'|_{\eta=-1} & \psi_2'|_{\eta=-1} \end{bmatrix} \begin{Bmatrix} \gamma_1 \\ \gamma_2 \end{Bmatrix} = -\begin{Bmatrix} \psi_0'|_{\eta=1} \\ 3/4\xi_\infty \delta_{nl} e^{3/2\xi_\infty} + \psi_0'|_{\eta=-1} \end{Bmatrix} \quad (27)$$

in which the prime indicates derivative with respect to the transformed spatial variable. It is worthwhile to point out that the left-hand-side matrices associated with the auxiliary problems are identical and remain unchanged throughout the course of simulation; hence, they can be decomposed to upper and lower matrices once and for all. Thus, the solution at any time level involves only backward and forward substitutions.

4. DRAG COEFFICIENT

One parameter often of interest in particle dynamics is the total drag force acting on the particle and in the direction opposite to the drop motion. For a droplet experiencing no interfacial mass transfer, the main contribution to the drag force is the pressure and the interfacial shearing force. When normalized with the inertial force ($\mu\rho U_\infty^2 R^2$), the equation for the net drag becomes

$$C_D = -2\int_{-1}^{1} \Pi|_{\eta=1}\zeta\, d\zeta - \frac{4}{\mathrm{Re}}\int_{-1}^{1} \Omega|_{\eta=1}(1-\zeta^2)^{1/2}\, d\zeta, \quad (28)$$

where Π is the pressure which can be obtained from the momentum equation. Since much algebraic manipulations are involved in deriving the equation for the pressure, detail is omitted. Nonetheless, it can be shown, in the form of surface pressure coefficient $K(\zeta)$ [7], that

$$K(\zeta) = \frac{\Pi|_{\eta=1} - \Pi_\infty}{1/2\rho U_\infty^2} = K(-1) - \frac{4}{\mathrm{Re}}\sum_{n=1}^{\mathrm{NL}}\left[\Omega_{n0} - \frac{2}{\xi_\infty}\sum_{l=0}^{\mathrm{NT}} \hat{G}_{0,l}^{(1)}\Omega_{nl}\right] \times [P_n(\zeta) - (-1)^n], \quad (29)$$

where Π_∞ is the free stream pressure and

$$K(-1) = 1 - \frac{2\xi_\infty}{\mathrm{Re}}\sum_{n=1}^{\mathrm{NL}} (-1)^n n(n+1)\int_1^{-1} \Omega_n(t,\eta)\, d\eta. \quad (30)$$

Upon integration, as indicated in (28), the term $K(-1)$ drops out and the final equation for the drag coefficient becomes

$$C_D = \frac{-8}{3\,\mathrm{Re}}\left(\Omega_{l0} + \frac{2}{\xi_\infty}\sum_{l=0}^{\mathrm{NT}} \hat{G}_{0,l}^{(1)}\Omega_{1l}\right), \quad (31)$$

which can easily be evaluated once the stream function components are obtained.

5. RESULTS AND DISCUSSION

In this section, the contents will be organized into two parts such that the accuracy as well as the adequacy of the Chebyshev expansion can be examined in detail followed by a discussion devoted to the main focus on flow about a spherical particle. To fulfill the first objective we shall investigate the convergence of a simple one-dimensional convective–diffusive–reactive equation of a scalar C written as

$$\frac{d^2C}{dr^2} + \lambda_1\frac{dC}{dr} + \lambda_2 C = 0, \quad r \in [0, 1], \quad (32)$$

with constant transport coefficients λ_1 and λ_2. The reason behind the selection of this equation is the fact that analytical solution is at hand, and moreover it resembles Eq. (20)

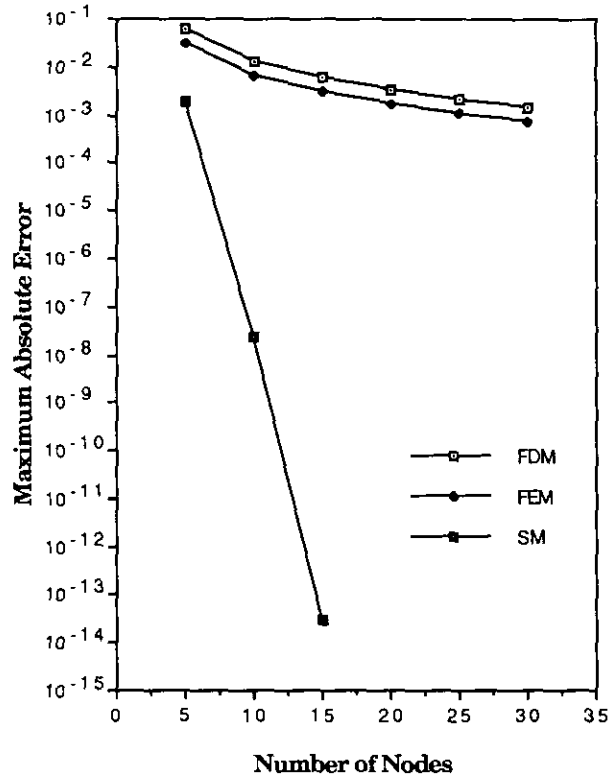

FIG. 1. Convergence rate of FDM, FEM, and SM.

TABLE I

Sensitivity of Drag Coefficient on ξ_∞

Re	$\xi_\infty = 3.0$	$\xi_\infty = 3.5$	$\xi_\infty = 4.5$	$\xi_\infty = 4.9$
1	14.212	13.927	13.847	13.840
20	1.374	1.371	—	—

with constant coefficients. In assessing the performance of the Chebyshev collocation against the traditional FDM and FEM methods, Eq. (32) is solved along with the boundary conditions $C(0)=0$ and $C(1)=1$ for several numerical grids. The results for $\lambda_1 = -3$ and $\lambda_2 = 2$ plotted in Fig. 1 again confirm the fact that both FDM and FEM generally require higher number of degrees of freedom than SM for a fixed level of accuracy. As indicated by the slope of the error curves, SM converges at a rate much faster than FDM and FEM, which are relatively insensitive with the number of nodes. This is true because $\log \|\text{Exact} - \text{Numerical}\|_\infty \sim \text{NT}$ for the SM method in contrast to log(NT) for FDM and FEM. It is rather unclear whether there is any increase/decrease in computational cost associated with the spectral algorithm in return for higher order of accuracy. However, a rough estimate about the magnitude of the computing time can be obtained through the following consideration: For example, by setting the absolute minimum allowable error to be 2×10^{-3}, the required number of nodal points are 6 for SM, 25 for FDM, and 17 for FEM. At this point, it is important to note that SM yields a full 6×6 matrix, while FDM and FEM produce tridiagonal matrices with 25 and 17 rows, respectively. Depending on the type of matrix solver involved and the available computer speed, these numbers can directly translated to operation counts; hence, the CPU time provided the preprocessing times are equal for all methods.

In what follows, we shall consider the unsteady developments of the flow around a sphere following a spatially uniform and impulsive start in an orientation from left to right. All the results generated are based on $\Delta t = 10^{-3}$ and $\{\varepsilon\} = \{10^{-3}, 10^{-3}\}$. With regards to the number of Legendre functions and the number of collocation points, there is no specific guideline for selecting those values because they depend on both the Reynolds number and the truncation radius; instead, they are determined iteratively. Table I gives the results of our convergence study on the drag coefficient as the truncation radius e^{ξ_∞} varies. On the basis of the findings in Table I, it is fair to conclude that $r_\infty \geqslant 90$ for $\text{Re} < 20$ and $r_\infty \geqslant 20$ for $\text{Re} \geqslant 20$. Due to the symmetry, only upper half of the flow domain is displayed in the illustrations.

Figure 2 provides a series of plots showing the steady-state velocity vectors ($t = 15$) for the case of a spherical particle being exposed to a moving ambience at $\text{Re} = 0.01$, 10, 50, and 200. Although the flow at small Reynolds number (Fig. 2a) is of very little interest in practice, it is one of the good tests that analytical solution is available for comparison. Mathematically speaking, when

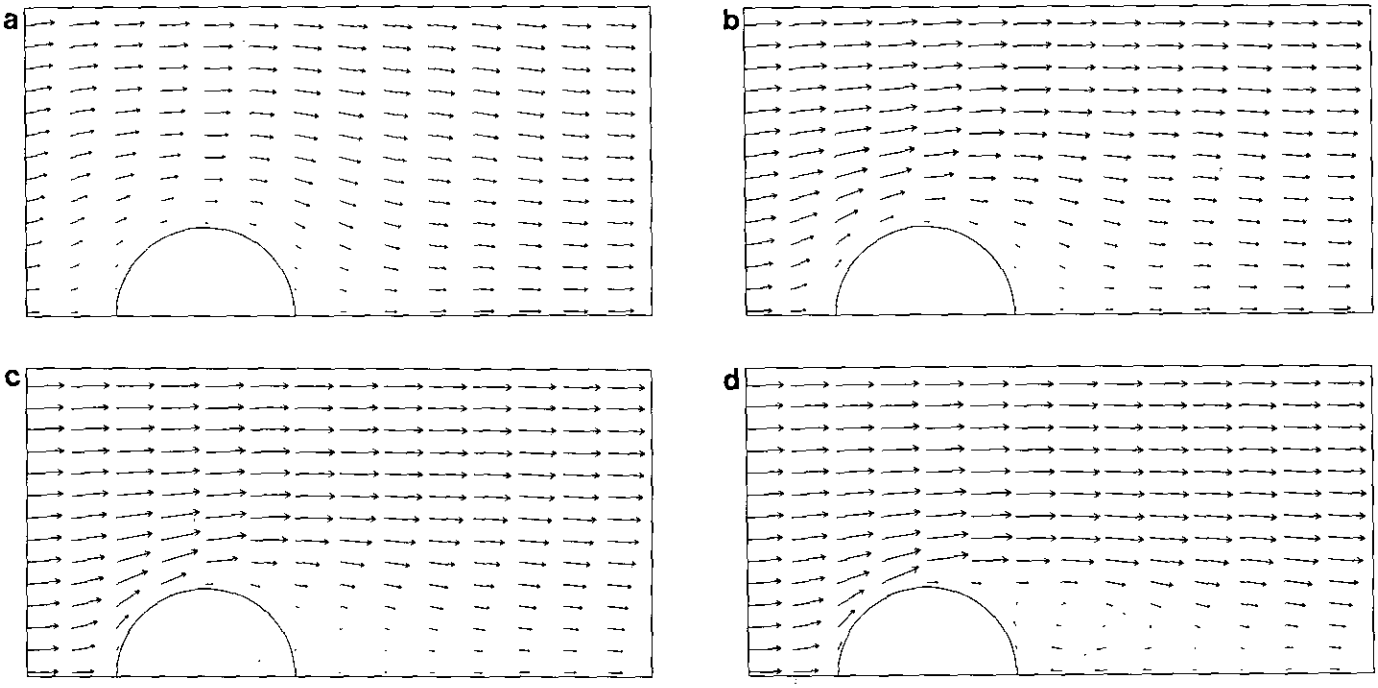

FIG. 2. Velocity vector at: (a) $t = 15$ for $\text{Re} = 0.01$; (b) $t = 15$ for $\text{Re} = 10$; (c) $t = 15$ for $\text{Re} = 50$; (d) $t = 15$ for $\text{Re} = 200$.

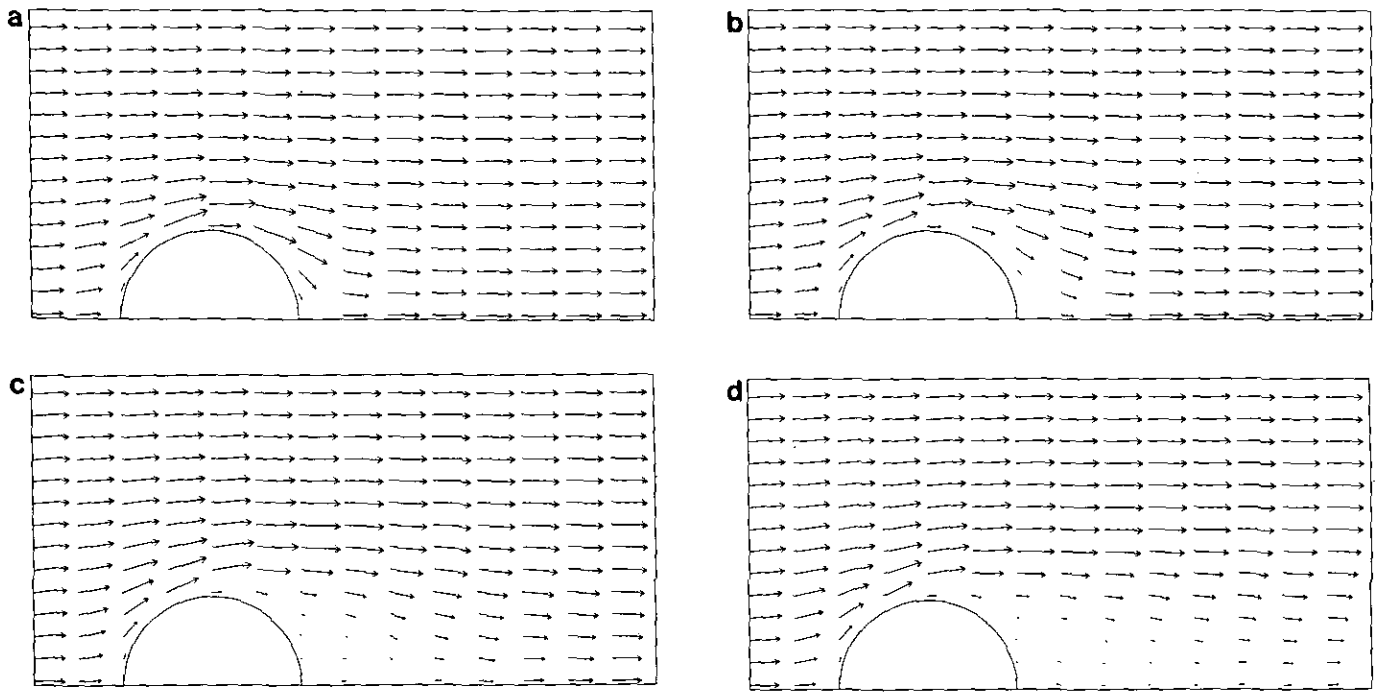

FIG. 3. Velocity vector at: (a) $t = 0.1$ for Re = 100; (b) $t = 5$ for Re = 100; (c) $t = 10$ for Re = 100; (d) $t = 15$ for Re = 100.

the convection term is discarded from the governing equation, the vorticity transport equation reduces to the Stokes' problem whose solution is invariant under reflection about both axes unless a nonuniform boundary condition is imposed. This required feature is clearly seen in Fig. 2a, where the deflection of the vectors is indeed symmetrical about the vertical axis $\theta = \pi/2$. Upon inspection of Fig. 2, it is seen that Fig. 2a possess a large region, indicated by the deflection of the velocity field, where viscous actions dominate. This characteristic is in agreement with the conventional order-of-magnitude analysis which had predicted this layer to be theoretically infinite for truly creeping flow (Re = 0). As the Reynolds number increases (see Fig. 2b), this layer thickness decreases and the fore-to-aft asymmetry, a precursor to the development of the wake behind the sphere, of the flow structure becomes more pronounced. Further increase in the Reynolds number causes the flow in the neighborhood of the rear stagnation point to reverse its direction. Figure 2c illustrates such feature. Depending on the strength of the main flow, the velocity in the recirculation zone could be low enough that the fluid trapped in that zone may be considered stagnant, as in Fig. 2c, where Re = 50, and could be high as in Fig. 2d, where Re = 200. Although the objective of this work is not to resolve the controversial issue about the onset of separation, an attempt has been made to validate the hypothesis, suggested by some fluid dynamicists, that separation would occur around Re = 20, but it was not observed in our numerical experiment, even though the calculation was extended up to $t = 15$. By comparing the flow structure and the drag coefficient at $t = 10$ and 15, we believe the steady state has been reached; therefore, such claim is inconclusive in this study.

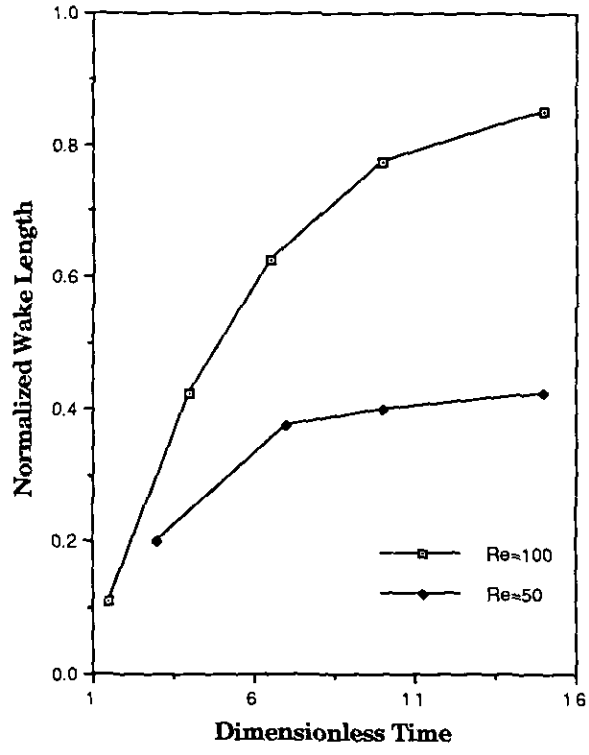

FIG. 4. Time history of wake length.

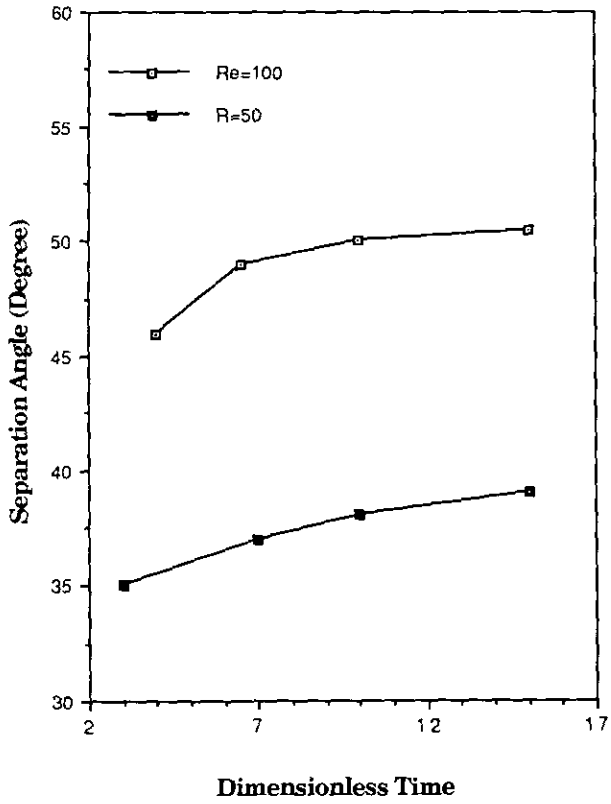

FIG. 5. Time history of wake angle.

Figure 3 shows the temporal development of the velocity field for Re = 100 depicted at $t = 0.1$, 1, 5, 10, and 15. At small times, the viscous effects are confined in a very small region so that most of the flow field behaves as it is a potential flow even at $t = 0.1$, Fig. 3a, at which much symmetry is still preserved. As time increases, the flow structure deforms in an asymmetrical fashion and a wake forms gradually (Fig. 3b). At a certain point in time, a recirculation zone is induced and the flow separates from the body of the sphere. Within the eddy, the fluid encounters an adverse pressure gradient which causes the flow to reverse its direction from the main stream and forces the entrained fluid to circulate in a clockwise manner (see Fig. 3c and 3d). Once an eddy is formed, its volume expands very rapidly at first and at slower rates as the flow moves toward the steady state. For instance, after about 1.5 units of dimensionless time since its inception, the wake length, defined as the distance from the rear stagnation point to the tip of the wake, is nearly one-half of the radius; and with four additional times units, the distance is almost double. If the Reynolds number is not high enough for the eddy to be detached from the sphere surface, the volume of the eddy widens and lengthens in the streamwise direction continually as time progresses and appears to attain a maximum value at steady state. This is substantiated by the data in Figures 4 and 5. Also evidenced from these figures is that the volume of the eddy increases significantly with Re.

TABLE II

Comparison of Wake Length and Separation Angle

	Wake length		Wake angle	
Re	Present	Ref. [14]	Present	Ref. [14]
50	0.43	0.42	139.0°	138.5°
100	0.85	0.86	129.5°	126.5°

TABLE III

Comparison of Drag Coefficient

Re	Present	Ref. [5]	Ref. [15, 16]
0.1	122.24	122.10	122.31
1	13.84	13.72	13.78
5	3.627	3.605	3.640
10	2.219	2.212	2.225
20	1.374	1.365	1.405
40	0.907	0.904	—
50	0.803	—	0.860
100	0.548	—	—
200	0.403	—	—
300	0.349	—	—

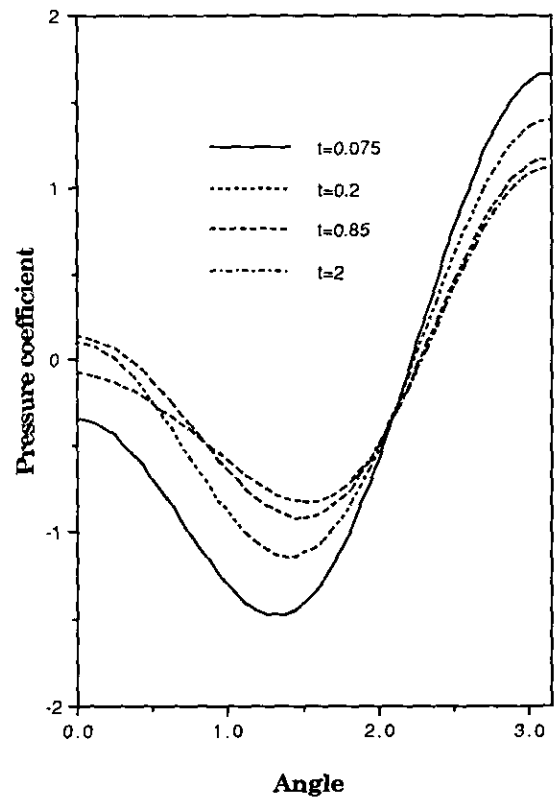

FIG. 6. Pressure coefficient along the sphere surface for Re = 100.

Although the above findings indicate a promising sign about the proper performance of the proposed numerical model, they need to be assessed quantitatively with existing solutions. As a first step in validating our numerical results, the time evolutions of the wake length and the angle of separation, measured from the front stagnation point, in Fig. 4 and 5 are extrapolated and compared along with those collected by Clift *et al.* [14] from a number of sources. Table II is a summary of our comparison where the magnitude of the error is within 2%. The incentive of this comparison on the wake length and separation angle is the elimentation of possible sources of error which may be accumulated during the integration of the pressure and the skin friction along the surface of the sphere.

Although it is believed that assessing the wake length and angle would give a direct indication of how well the numerical scheme performs locally, it is also of important to compare the drag coefficient. Table III tabulates the present predictions for several values of Reynolds numbers, ranging from 0.1 to 300, along with the results of Dennis and Walker [5] and of Oliver and Chung [15, 16]. It appears that the combined Galerkin/collocation spectral method is capable of predicting the drag force accurately. In computing these late time drag coefficients, the solution is allowed to advance in time until the change in the drag coefficient is less than 10^{-5}.

It is noticeable from the above table that neither Dennis and Walker [5] nor Oliver and Chung [15, 16] provided the drag coefficient for Re = 100, 200, and 300. To verify these values, we compared them against those computed from the correlation of Schiller and Nauman [17] documented in the book by Clift *et al.* [14]. According to Clift and his associates, the range of deviation of the Schiller and Nauman empirical equation is from +5 to −4%, and seems to be the best, for Re < 800, among the correlations they documented. The values calculated from this correlation were 0.546, 0.403, and 0.342, which agree exceptionally well with our results.

As far as the transient nature of the flow is concerned, much of the information from the work of Dennis and Walker [7] is relevant for comparison with ours. However, because their data were presented in graphical form, it is difficult to perform a numerical assessment. For qualitative comparison purposes, the time response of the surface pressure and vorticity for Re = 100, and of the drag coefficient, are presented in Fig. 6, 7, and 8, respectively. These curves are comparable to those of Dennis and Walker [7] both qualitatively and quantitatively, except at early times where our predictions are somewhat higher, especially near the front stagnation point. Another good test is the comparison of the separation time. By extrapolating the wake lengths, the separation time for Re = 50 and 100 is estimated to be about 1.5 and 0.8, respectively, and these are in the same bulk part of Dennis and Walker calculations [7].

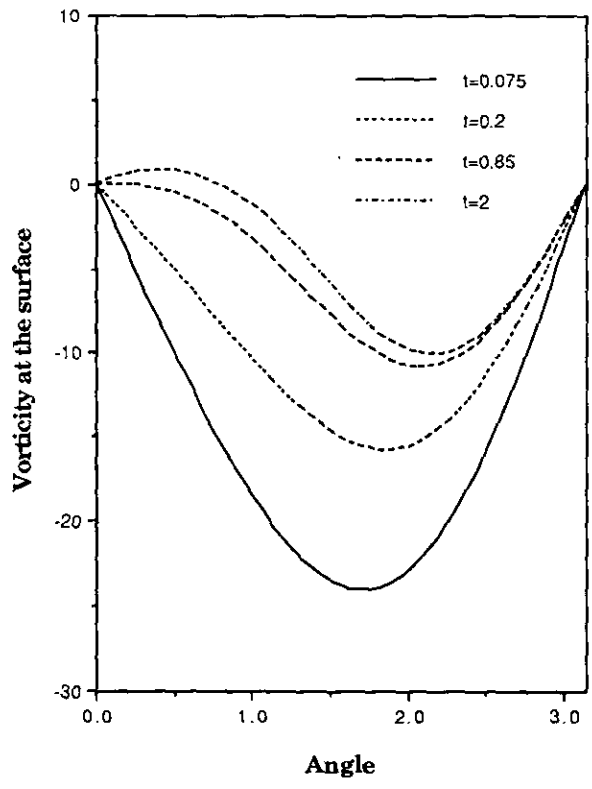

FIG. 7. Vorticity distribution along the sphere surface for Re = 100.

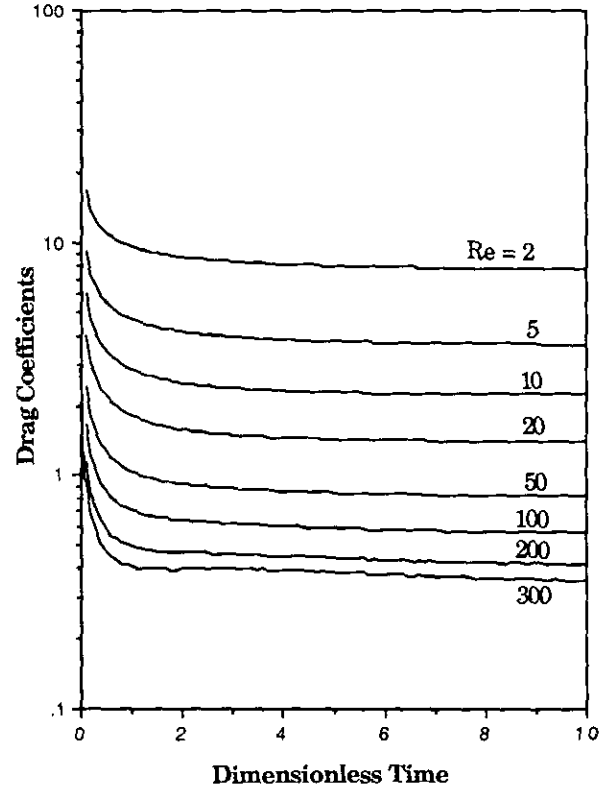

FIG. 8. Time history of drag coefficient.

Despite the lack of the available transient data, we are confident about the present numerical model. Such conclusion comes from good agreement of local and global data as well as limited transient data.

6. CONCLUDING REMARKS

The proposed Chebyshev–Legendre spectral model has been tested for the flow associated with a spherical particle. The following conclusions are drawn:

1. The present SM model is especially well suited for axisymmetric flow associated with spherical bodies. It is easily be extended to two-phase flow problems in which the continuous and the dispersed media may be either gas or liquid. These studies are currently underway.

2. Accuracy associated with the proposed method is likely an order higher than FDM and FEM. However, the computational cost is probably higher because the matrices are unbanded. Nonetheless, the computing time does not seem to be a concern because of the recent advances in computer technology, both in hardware and software. Moreover, accuracy is sometimes more important than computing power in many problems such as transition and turbulent flows.

3. The use of the Galerkin procedure is very appropriate to the type of flows undertaken in this study because it reduces the dimension of the problem by one. Such a technique also weakens the effects of aliasing errors which are known to exist in pseudospectral methods.

ACKNOWLEDGMENTS

The authors are indebted to Drs. Richard W. Johnson and Seungho Paik of the Computational Fluid Dynamics Unit, and Mr. Richard Martineau of the Geosciences Unit of EG & G Idano, Inc., for their review and helpful comments. This work is performed under the auspices of the U.S. Department of Energy, contract DE-AC07-76-ID01570, and was supported in part by the INEL Long-Term Research Initiatives Program.

REFERENCES

1. C. A. J. Fletcher, *Computational Galerkin Methods* (Springer-Verlag, New York, 1984).
2. A. T. Patera, *J. Comput. Phys.* **54**, 468 (1984).
3. C. Canuto, M. H. Hussaini, A. Quarteroni, and T. A. Zang, *Spectral Methods in Fluid Dynamics* (Springer-Verlag, New York, 1988).
4. H.-C. Ku and D. Hatziavramidis, *Comput. Fluids* **13**, 99 (1985).
5. S. C. R. Dennis and J. D. A. Walker, *J. Fluid Mech.* **48**, 771 (1971).
6. S. C. R. Dennis, S. N. Singh, and D. B. Ingham, *J. Fluid Mech.* **101**, 257 (1980).
7. S. C. R. Dennis and J. D. A. Walker, *Phys. Fluids* **15**, 517 (1972).
8. S. C. R. Dennis and D. B. Ingham, *Phys. Fluids* **22**, 1 (1979).
9. M. Rottenberg, R. Bivins, N. Metropolis, and J. K. Wooten, *The 3-J and 6-J Symbols* (MIT Press, Cambridge, 1959).
10. H. D. Nguyen, S. Paik, and J. N. Chung, submitted for publication.
11. S. C. R. Dennis and L. Quartapelle, *J. Comput. Phys.* **52**, 448 (1983).
12. A. Chaouche, A. Randriamampianina, and P. Bontoux, *Comput. Methods Appl. Mech. Eng.* **80**, 237 (1990).
13. T. N. Phillips and I. M. Soliman, *Numer. Methods Partial Diff. Eqn.* **1**, 9 (1991).
14. R. Clift, J. R. Grace, and M. E. Weber, *Bubbles, Drops, and Particles* (Academic Press, New York, 1978).
15. D. L. R. Oliver and J. N. Chung, *J. Fluid Mech.* **154**, 215 (1985).
16. D. L. R. Oliver and J. N. Chung, *J. Fluid Mech.* **177**, 1 (1987).
17. L. Schiller and A. Z. Nauman, *VDI Z.* **77**, 318 (1933).